Appl. Phys. B (2006)
DOI: 10.1007/s00340-006-2426-4

**Applied Physics B**
**Lasers and Optics**

J.J. MCFERRAN✉
W.C. SWANN
B.R. WASHBURN
N.R. NEWBURY

# Suppression of pump-induced frequency noise in fiber-laser frequency combs leading to sub-radian $f_{ceo}$ phase excursions

Optoelectronics Division, National Institute of Standards and Technology, 325 Broadway, MS 815.03, Boulder, Colorado 80305, USA

**Received: 2 June 2006/Revised version: 1 August 2006**


**ABSTRACT** We discuss the origins and the suppression of the large frequency jitter on the carrier-envelope offset frequency ($f_{ceo}$) of fiber-laser frequency combs. While this frequency noise appears most prominently on $f_{ceo}$, its effects are felt across the frequency comb and it is a potential limiting factor in applications of fiber-laser frequency combs. Here we show that its origin lies in the white amplitude noise of the pump laser output. We dramatically reduce this noise by operating the pump laser in a lower-noise state, i.e. at higher pump current, and by more aggressively feeding back to the pump current with an optimal feedback network. We demonstrate instrument-limited $f_{ceo}$ linewidths and an integrated $f_{ceo}$ phase jitter of 1 rad.

**PACS** 42.55.Wd; 42.62.Eh; 42.60.Lh; 06.30.Ft

## 1 Introduction

The versatility and use of optical frequency combs will increase dramatically as they become easier to operate, more compact and portable, operational over longer time periods, less power consuming and more cost effective. Fiber-based frequency combs demonstrate superiority in the majority of these attributes compared to solid-state/discrete-optic-based frequency combs. Since the first direct detection of the offset frequency beat [1, 2], the development of fiber-laser-based frequency combs has moved rapidly from the first self-referenced phase-locked comb [3] to compact turnkey systems [4, 5], systems with coverage in the visible [6–8], robust two-branch combs [9], variable repetition rate combs [10], and, of course, applications of combs to metrology [9, 11] as well as other areas [12]. In addition to these practical demonstrations, the basic theory of phase locking of the combs is also well understood [13, 14]. However, one drawback of fiber combs compared to solid-state systems is the high level of frequency noise associated with comb elements in the wings of the comb, in particular the noise of the related carrier-envelope offset (CEO) frequency [1, 3, 4, 9, 10]. The noise of the offset frequency in fiber systems has been a cause for concern, because it can place a limit on optical frequency metrology applications and can potentially limit time-domain applications that require low jitter on the carrier-envelope offset phase. There have been conflicting reports and conjectures on the origin of $f_{ceo}$ noise. The simultaneous observation of an $f_{ceo}$ beat width of a few hundred kHz and a comb linewidth of tens of kHz near 1 μm might lead one to conclude naively that the comb linewidth at 2 μm must be very broad in order to explain the broad $f_{ceo}$ beat, and therefore that there is some form of excess noise generated in the nonlinear fiber during supercontinuum formation. However, recently Benkler et al. [15] demonstrated that the noise of $f_{ceo}$ and the repetition rate of the femtosecond laser are highly correlated, implying that the comb fluctuates in frequency in a breathing-like manner about a fixed frequency, $f_{fix}$, that is not too far from the carrier frequency (see further discussion below). The same authors suggested that the origin of technical noise might be pump current fluctuations. Such a breathing motion is also to be expected from the comb response to variations in the pump power [13, 14]. In a recent letter [16], and in greater depth than given here, we presented data substantiating this explanation. We found that the primary cause of frequency noise associated with the offset frequency is the relative intensity noise of the pump laser driving the femtosecond laser. This noise causes an approximately linear increase in the linewidth of the comb elements as one moves toward either edge of the comb. Furthermore, we show that the in-loop linewidth of $f_{ceo}$ can be reduced to less than 1 Hz with an integrated phase noise of $\sim 1$ rad using pump current feedback with a servo bandwidth of $\sim 80$ kHz. Although tests here have been conducted on a single laser system, the results are general and should apply to any fiber-based comb that is mode locked through nonlinear-polarization rotation [17] (and similarly for other types of mode-locked lasers). It is interesting that similar narrow linewidth $f_{ceo}$ beats have been observed in another fiber-laser comb system [5, 18] using a femtosecond fiber laser that relies on a saturable absorber for mode locking.

This paper is divided into five main sections. Section 2 describes the fiber-based frequency comb, including the femtosecond laser, the amplification stage, and the nonlinear interferometer used to detect the carrier-envelope offset frequency. Section 3 is divided into three parts: the first summarizes measurements of the offset and repetition frequency noise dependence on the intensity noise of the pump laser driving the femtosecond laser, the second goes through a step

✉ Fax: +61-8-6488-7364, E-mail: jmcferran@physics.uwa.edu.au

by step approach linking the intensity noise of the pump laser to the frequency noise on the comb using the measured comb response, and the third provides a discussion of the relationship between the noise spectral density of $f_{ceo}$ and its associated linewidth. Section 4 discusses the frequency noise across the comb caused by the pump intensity noise. Section 5 describes how the residual phase noise of $f_{ceo}$ can be suppressed to $\sim 1$ rad using a fast servo in conjunction with passive noise suppression brought about by reducing the intensity noise of the pump laser.

## 2 Frequency comb and $f_{ceo}$ generation

The general layout of the frequency comb apparatus is depicted in Fig. 1. A femtosecond laser (fs laser) operating in the stretched-pulse mode [17, 19], which contains an open-air section, lies at the heart of the frequency comb. Its pulses are amplified in an Er-doped fiber amplifier (EDFA) before entering a short length of dispersion-shifted, germanosilicate highly nonlinear fiber (HNLF) [20]. The subsequent octave-spanning comb then allows for photodetector extraction of the offset frequency signal. The fs laser is composed of 1.69 m of erbium fiber ($\beta_2 \sim 31$ ps$^2$/km), 2.45 m of single-mode fiber ($\beta_2 = -21$ ps$^2$/km), and a 0.16-m open-air section composed of optics for polarization control and unidirectional operation of the fs laser. A Glan-laser prism provides the main output coupling from the laser. The erbium fiber in the cavity is pumped with 1480-nm light coupled in via a 1480/1550 nm wavelength-division multiplexer (WDM) to produce lasing centred near 1560 nm. The 1480-nm pump source is a Fabry–Pérot diode laser that is Bragg-grating stabilized. The variable attenuator following the pump laser is used to control the relative-intensity noise of the pump laser acting on the fiber laser (see further discussion below). Upon mode locking of the fiber laser the mean output optical power is $\sim 8$ mW and it generates a repetition-frequency signal at 50 MHz. Through the course of this work the repetition rate, $f_r$, of the laser changed from 49.3 MHz to 50.1 MHz; where the difference is important, the more precise $f_r$ value will be stated. Up to 80% of this optical power is coupled into a single-mode fiber before being directed to the EDFA. The spectral width of the light exiting the fs laser is 80–85 nm wide (the corresponding transform-limited pulse width for a Gaussian-shaped pulse is $\sim 45$ fs). This broad spectral width and the lack of Kelly sidebands on the spectrum indicate that the laser is acting in the stretched-pulse mode, where the net cavity dispersion, $\beta_2$, is close to zero but slightly positive. Such a broad spectrum requires careful selection of fiber optic lengths before and after the amplifier to produce single narrow pulses suitable for comb broadening in highly nonlinear fiber. At present the pulses from the fiber laser pass through a temporal waist of 80 fs before expanding to approximately 600 fs at the input to the EDFA. The amplifier is composed of 0.95 m of Er-doped fiber and is solely backward pumped with $\sim 250$ mW of 1480-nm radiation. 45 cm of single-mode fiber then compresses the pulse width to $\sim 55$ fs before entering the HNLF (the spectral width exiting the EDFA is $\sim 110$ nm). The mean power required for an octave-wide spectrum is about 80 mW with a corresponding peak power of $\sim 25$ kW, which is easily obtained from the EDFA. The broadened comb generated by the HNLF extends from $\sim 960$ nm to $\sim 2200$ nm. Radiation at 2060 nm is chosen for second-harmonic generation in the $f$–$2f$ nonlinear interferometer used to extract the carrier-envelope offset frequency signal, $f_{ceo}$. Both a dual-arm interferometer and a collinear interferometer [4] have been used for generating $f_{ceo}$ signals.

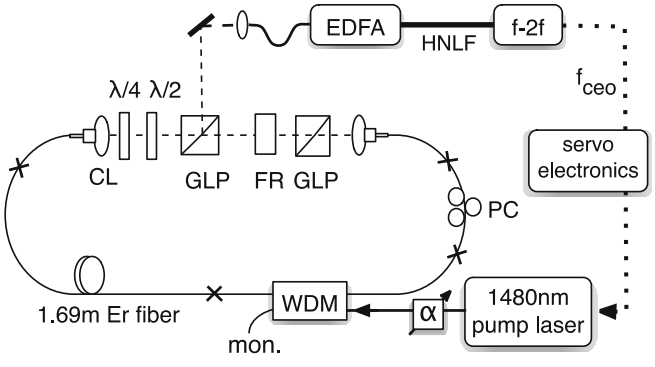


**FIGURE 1** Broad layout of the frequency comb apparatus. The laser operates in the stretched-pulse regime with a repetition frequency of 50 MHz. *Unlabelled solid line* represents single-mode fiber. The $f_{ceo}$ servo is not operating when the free-running noise measurements are taken. CL, coupling lens; GLP, Glan-laser prism; FR, Faraday rotator; PC, polarization controller; WDM, wavelength-division multiplexer; EDFA, Er-doped fiber amplifier; HNLF, highly nonlinear fiber; $\alpha$, variable attenuator

## 3 Influence of pump laser noise on the comb

In this paper we assert that the majority of the noise observed on the $f_{ceo}$ signal is derived from the relative-intensity noise (RIN) of the pump laser driving the fiber femtosecond laser. Two approaches have led us to this conclusion. One is the direct measurement of the noise (defined below) of $f_{ceo}$ as a function of the pump laser RIN. The other establishes a series of links between the RIN of the pump laser, the noise on the repetition-rate signal, and the noise on the CEO frequency signal. These links include: (1) a relationship between the RIN of the pump laser and the RIN of the fs laser, (2) a measurement of the conversion of amplitude modulation (AM) of the pump laser to frequency modulation (FM) of the repetition rate and offset frequency of the fs laser [13], and (3) combining these AM to FM response measurements with the measured laser RIN to predict the observed frequency noise on elements of the frequency comb. These aspects have been summarized with the block diagram of Fig. 2. The nomenclature in italics will be used later in the text.

For the duration of this paper the frequency noise of a particular carrier signal is implied to be equal to $S_f(\nu) = \nu^2 S_\varphi(\nu)$, where $S_\varphi(\nu)$ is the power spectral density (PSD) measured in rad$^2$ rms/Hz bandwidth and $\nu$ is the Fourier frequency. Here we consider $S_f(\nu)$ to be the total frequency noise mapped onto one side of the carrier, i.e. the one-sided PSD [21]. Since the discussion of noise will be restricted to $S_f(\nu)$ rather than $S_\varphi(\nu)$, the subscript $f$ will often be replaced with labels representing the repetition rate, the offset frequency, or the mode number $n$ of the frequency comb and its associated wavelength. The term 'frequency noise' may also refer to the

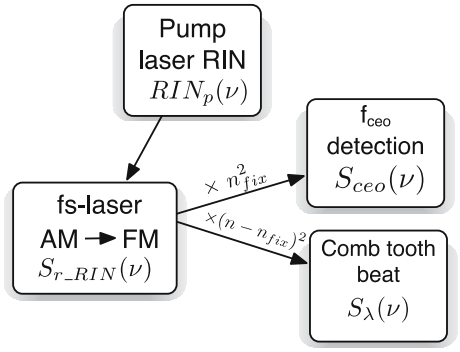


**FIGURE 2** Block diagram illustrating the relationship between noise terms in the overall experiment, along with the associated nomenclature. $RIN_p$ = relative-intensity noise of the pump laser, $S_{r\_RIN}$ = frequency noise power spectral density (PSD) of $f_r$, $S_{ceo}$ = frequency noise PSD of $f_{ceo}$, $S_\lambda$ = frequency noise PSD of a comb tooth at a wavelength $\lambda$, $\nu$ = Fourier frequency

closely related noise parameter, the linewidth ($\Delta f$), describing the full width at half-maximum of the field spectrum of a particular signal.

### 3.1 *Measured effect of pump laser noise on the offset frequency and repetition frequency*

We first present direct measurements of the $f_{ceo}$ noise, the $f_r$ noise, and the pump laser noise. The pump noise is characterized by the spectral density of the relative-intensity noise defined as the squared fractional change in pump power (the units used here will be dBc/Hz ≡ dB AM rms$^2$/Hz). To adjust the RIN level, the 1480-nm-wavelength pump laser was operated at a selection of different forward currents, while the level of optical attenuation was changed to maintain identical power incident on the fs laser. The limiting current was 1 A for the laser diode current supply (note that the specified operating current was 1.1 A). Figure 3 illustrates the RIN dependence on the pump current. A change in pump laser current has a clear influence on the relative-intensity noise of the emitted light. The measured pump RIN is well above the RIN of the pump current supply, which when measured ranged between −138 and −148 dB c/Hz for currents between 310 mA and 1 A, respectively. The pump RIN levels of Fig. 3 were similarly observed for a 980-nm pump diode laser. This high level of RIN from Bragg-grating-stabilized Fabry–Pérot diode lasers is known from work on Raman amplifiers [22], although not well understood. It may be associated with optical feedback from the fiber grating. There are distributed feedback diode lasers that have significantly lower RIN levels although, unfortunately, they are not at present commercially available at the appropriate power levels for driving a fiber laser.

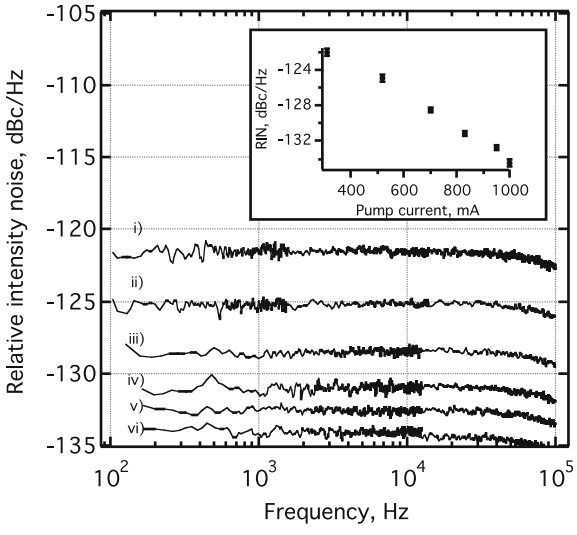


**FIGURE 3** Pump laser relative-intensity noise for different pump currents as a function of Fourier frequency. The pump laser is a Fabry–Pérot diode laser that is Bragg-grating stabilized to 1480 nm. (i) 310 mA, (ii) 520 mA, (iii) 700 mA, (iv) 830 mA, (v) 950 mA, (vi) 1 A. *Inset*, mean (white) RIN vs. pump current

For the measurements of the linewidth of $f_{ceo}$, six rf spectra were recorded for each pump laser noise setting, their full width half-maximum (FWHM) linewidths determined from Lorentzian line shape fits, and the mean value deduced. The relationship between $f_{ceo}$ linewidth and RIN, along with the corresponding pump laser current, is shown in Fig. 4 (the error bars correspond to the standard deviation of linewidths of the six measurements at each current setting). There is a clear reduction of $f_{ceo}$ noise with increasing current until the higher pump currents are reached. Increases in current beyond 1 A were made on a separate occasion using a different laser diode driver, but linewidths lower than those shown here were not achieved.

To accompany the linewidth measurements, the noise power spectral density of $f_{ceo}$ was recorded for the same pump current levels above, again, with the appropriate attenuation to maintain the same power incident on the cavity (nearest the mode-locking pump power threshold, the current was increased from 310 mA to 320 mA to reduce the risk of mode-locking failure). The offset frequency signal, divided by 256, was internally demodulated by a FFT spectrum analyser to compose the one-sided PSD. Figure 5 shows the $f_{ceo}$ PSDs with the division factor of 256 accounted for. Again there is a very obvious decline in frequency noise as the pump laser is driven at higher currents (closer to its nominal oper-

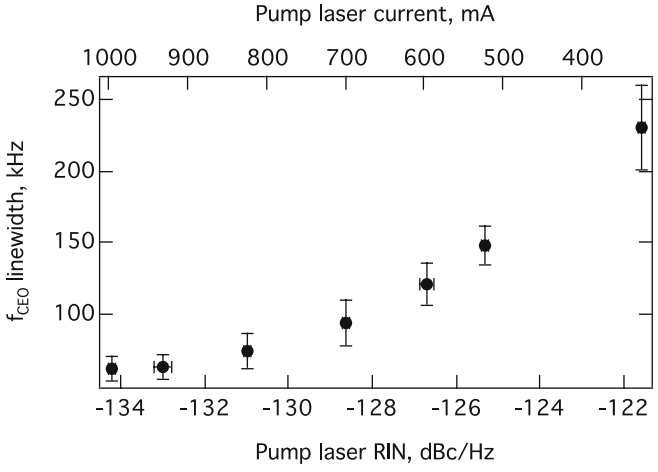


**FIGURE 4** FWHM linewidth of $f_{ceo}$, using Lorentzian line shape fitting, as a function of pump laser current and the corresponding relative-intensity noise

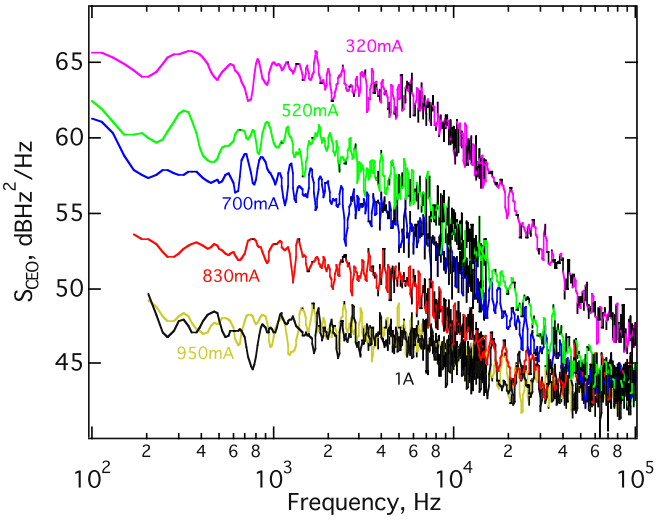


**FIGURE 5** Noise power spectral density (one-sided) of $f_{ceo}$ for a range of pump laser currents. The optical power incident on the femtosecond laser is held constant by using appropriate attenuation of the incident light

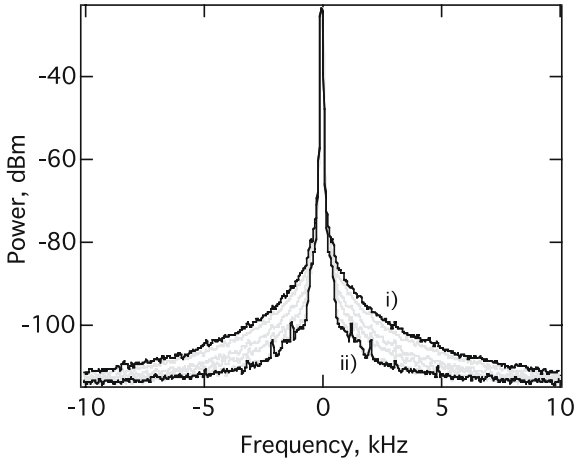


**FIGURE 6** Field spectra of the 200th harmonic of the repetition frequency (offset to 0 Hz) for (i) 320-mA and (ii) 1000-mA pump currents. The *gray traces* are field spectra recorded at intermediate pump current levels. The resolution bandwidth is 300 Hz

ating current), and thus at lower levels of RIN. At the highest currents, the frequency noise flattens to an approximate white-noise floor at a level of $\sim 43$ dB Hz$^2$/Hz. Such a white-noise floor is expected from the quantum-limited noise on fiber lasers [23–25], although the observed level of white noise appears higher than expected. This additional noise is presumably responsible for the lower limit on the linewidth observed in Fig. 4 at high pump currents. The relationship between $S_{ceo}$ and $f_{ceo}$ linewidth is discussed in Sect. 3.3, and the cause of the spectral density roll-off is addressed in Sect. 3.2.

The repetition frequency is also affected by the noise on the pump laser. The $-3$ dB linewidth of the repetition frequency is mainly set by environmental perturbations that change the length of the cavity. However, in the wings of the line shape we see a clear reduction in noise with decreasing pump RIN as shown in Fig. 6. Note the presence of what appear to be acoustic resonances when the laser RIN becomes less dominant.

### 3.2 *Pump intensity noise conversion to $f_r$ and $f_{ceo}$ noise*

The data presented in Sect. 3.1 shows that the noise on $f_{ceo}$ and $f_r$ depends upon the noise level of the pump laser, indicating that there is a close relationship between frequency changes in $f_{ceo}$ and $f_r$ and changes in pump power. This relationship is not unexpected, since the dependence of both $f_{ceo}$ and $f_r$ on the pump laser has been discussed in [13, 14]. Perturbations that affect the cavity round-trip time, and thus $f_r$, include the resonant gain contribution, spectral shifts, third-order dispersion, and self-steepening. The same perturbations will also affect $f_{ceo}$ along with the added contribution from self-phase modulation. For the discussion here, a separation between the different phenomena is not required; rather, we note that pump power changes will act in a deterministic way to change both $f_{ceo}$ and $f_r$. Therefore, noise on the pump power will lead to linearly correlated noise on $f_{ceo}$ and $f_r$. Because this noise is linearly correlated there will be one comb tooth frequency $f_n = n f_r - f_{ceo}$ for which the noise is cancelled (i.e. $\delta f_{n_{fix}} = n\delta f_r - \delta f_{ceo} = 0$). This comb tooth is referred to as the fixed point for the comb [15, 26], and is denoted $n_{fix}$ with frequency $f_{fix}$. This fixed point does not have to occur within the bandwidth of the frequency comb output; in principle, it can reside at a comb tooth of $n = 0$ or $n \to \infty$, but under normal operating conditions it happens to reside near the centre of the laser spectral output [13, 14]. In addition, $f_{fix}$ experiences a dependence on pump laser power driving the cavity, but throughout this paper the pump power incident on the fs laser cavity is constant and therefore the fixed point is likewise constant. In response to pump power fluctuations the comb will perform breathing motion about this fixed point [16]. Below, we develop this picture more fully to explain quantitatively the data of Sect. 3.1.

Taking a step by step approach of demonstrating a relationship between the RIN of the pump laser and the noise of $f_{ceo}$ and $f_r$, we begin with a comparison of RIN measurements between the pump laser and the femtosecond laser. The RIN levels of each are shown in Fig. 7 for two current settings with appropriate optical attenuation to maintain equal power driving the fiber laser. The roll-off at $\sim 7$ kHz seen in the AM behaviour of the fs laser is expected, resulting from a combination of the laser dynamics and the gain response time of the erbium-doped fiber [13, 14]. Prior to the roll-off, the RINs of the pump laser and fs laser are seen to be similar, aside from the noise generated by environmental perturbations. The relationship between fs-laser RIN and pump RIN can thus be described by

$$\mathrm{RIN_l}(\nu) = \varepsilon \left( \frac{\mathrm{RIN_p}}{1 + (\nu/\nu_{3\,\mathrm{dB}})^2} \right) , \qquad (1)$$

where $\mathrm{RIN_p}$ and $\mathrm{RIN_l}$ are the relative intensity noise of the pump laser and fs laser, respectively, and $\nu_{3\,\mathrm{dB}}$ is the $-3$ dB roll-off frequency of the fs laser's AM response. The factor $\varepsilon \sim 1$ reflects the fact that the pump spectrum is not completely matched to the absorption band of the erbium fiber; there is a strong lasing peak at 1480 nm and a weaker spontaneous emission peak at 1460 nm. Differential absorption of the Er gain medium between the 1460- and 1480-nm peaks alters the effective pump noise RIN in a way very akin to mode partition noise except on a larger wavelength scale.

This intensity noise on the pump will cause frequency fluctuations of the laser repetition rate (essentially there is AM to FM conversion in the femtosecond laser.) The AM to FM sensitivity, quantified by $P\,\mathrm{d}f_\mathrm{r}/\mathrm{d}P$, is easily measured at low Fourier frequencies [13] by monitoring changes in the repetition rate as the pump laser power is modulated (typically with a square waveform to avoid the influence of thermal delay). The value of $\mathrm{d}P$ is measured as a peak-to-peak voltage from a photodetector with a portion of the pump laser light incident upon it, while the DC level generates $P$. We find $P\,\mathrm{d}f_\mathrm{r}/\mathrm{d}P = -320 \pm 8$ Hz for frequencies below 10 Hz.

From predictions and suggestive measurements in [13] the response of the repetition frequency should fall off with the same $-3$ dB roll-off frequency as for the laser RIN response. The response function was measured out to 10 kHz by detecting a phase-sensitive signal derived from $f_\mathrm{r}$ and simultaneously modulating the pump current. A $-3$ dB roll-off was observed at $\sim 7$ kHz similar to that seen in Fig. 7. Tying together the RIN of the fs laser, the above response function, and the frequency noise of $f_\mathrm{r}$, we have

$$S_{\mathrm{r}_m}(\nu) = m^2 \left(\frac{P\,\mathrm{d}f_\mathrm{r}}{\mathrm{d}P}\right)^2 \mathrm{RIN_l}(\nu)\,, \tag{2}$$

where $S_{\mathrm{r}_m}(\nu)$ is the frequency noise of the $m$th harmonic of $f_\mathrm{r}$ and we consider $P\,\mathrm{d}f_\mathrm{r}/\mathrm{d}P$ to be evaluated at $\nu = 0$ Hz. Incorporating (1), this extends to

$$S_{\mathrm{r}_m}(\nu) = m^2 \left(\frac{P\,\mathrm{d}f_\mathrm{r}}{\mathrm{d}P}\right)^2 \left(\frac{\varepsilon\,\mathrm{RIN_p}}{1+(\nu/\nu_{3\,\mathrm{dB}})^2}\right)\,. \tag{3}$$

In Fig. 8, we can compare the predicted repetition rate frequency noise to the measured repetition rate noise for the 200th harmonic of $f_\mathrm{r}$ ($S_{\mathrm{r}_{200}}$). The frequency range of interest is that beyond 500 Hz, since, as we will see later, it is the multiplication of this noise that predominates in the wings of the frequency comb. The measured noise of $S_{\mathrm{r}_{200}}$ has contributions from the microwave synthesizer used to make the measurements for $\nu > 7$ kHz. The white phase noise of the synthesizer is shown as the dotted line in Fig. 8 (it has white frequency noise below 1 kHz). This has been subtracted from the measured PSD to produce trace 1. We see that the level of noise calculated from (2) overlaps with the measured $f_\mathrm{r}$ frequency noise beyond 500 Hz and out to as far as the measurement allows. Below 200 Hz, $S_{\mathrm{r}_{200}}$ is dominated by environmental effects and diverges from the predictions of (2) (the environmental noise on the repetition rate will dominate the frequency fluctuations of the comb tooth at and near the fixed point of the comb; see Sect. 4). Now let us consider the modulation of a comb tooth near zero frequency (i.e. $f_\mathrm{ceo}$). We have measured the AM to FM response for $f_\mathrm{ceo}$ to find $P\,\mathrm{d}f_\mathrm{ceo}/\mathrm{d}P = -1.30 \pm 0.02$ GHz at low Fourier frequencies. In this case the response is much more clearly observed because of the greater sensitivity of $f_\mathrm{ceo}$ than $f_\mathrm{r}$ to pump power changes. The predicted frequency noise of $f_\mathrm{ceo}$ due to pump RIN is found by squaring the AM to FM response and multiplying by the laser RIN, as done similarly in (2):

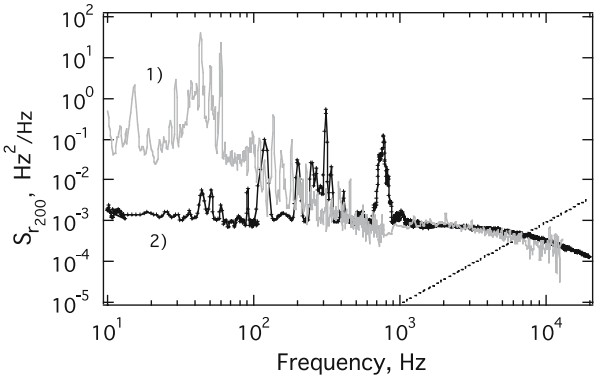


**FIGURE 8** Comparison between: (1) the frequency noise of the 200th harmonic of the repetition frequency of the fiber laser and (2) the AM-to-FM converted amplitude noise of the fiber laser for the same RIN (pump current = 520 mA), computed using (2). *Dotted line*, level of white phase noise of the microwave synthesizer used in the measurement of trace 1

$$S_\mathrm{ceo}(\nu) = \left(\frac{P\,\mathrm{d}f_\mathrm{ceo}}{\mathrm{d}P}\right)^2 \mathrm{RIN_l}(\nu)\,. \tag{4}$$

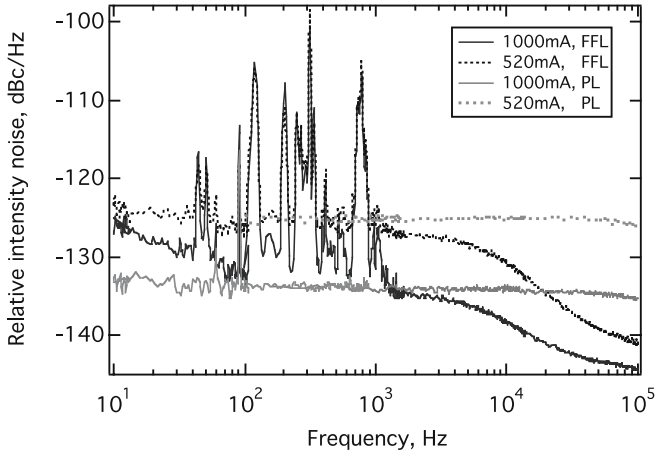


**FIGURE 7** Relative-intensity noise of the 1480-nm pump laser and the fiber laser at two current levels. The fiber laser is driven by the same pump power in each case through appropriate optical attenuation. PL, pump laser; FFL, femtosecond fiber laser

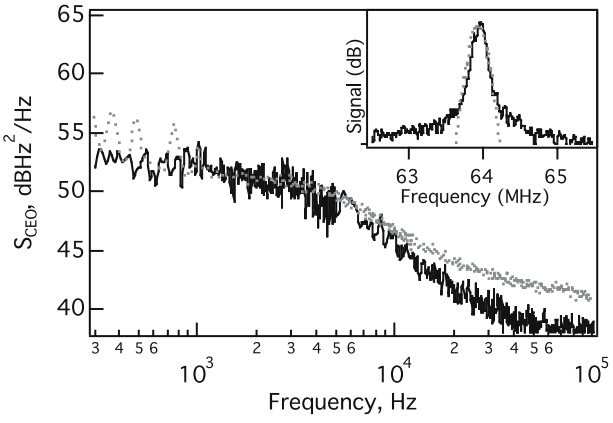


**FIGURE 9** The measured $S_\mathrm{ceo}$ (*solid line*) and $S_\mathrm{ceo}$ calculated from scaling the measured laser RIN (*dashed gray line*). *Inset*: the measured $f_\mathrm{ceo}$ line shape (*solid line*) and the calculated line shape (*dashed gray line*) obtained from only the pump-induced frequency noise

Analogous to Fig. 8, Fig. 9 (equivalent to Fig. 3 of [16]) shows a comparison between the measured $f_{\mathrm{ceo}}$ noise and the noise calculated from (4) and the measured laser RIN. Good agreement is seen between the two traces. The higher elevation of the scaled RIN trace at higher frequencies is due to a RIN measurement noise floor. Again we see a $-3$ dB roll-off at $\sim 7$ kHz, similar to $f_{\mathrm{r}}$ response measurements.

### 3.3 *Linewidth and power spectral density of $f_{ceo}$*

In Sect. 3.1 we presented both linewidth data and noise PSD data (Figs. 4 and 5, respectively). Section 3.2 discussed only the noise PSD. Here we discuss the relationship between this noise PSD and the linewidth. Figure 10 plots the same measured linewidths as in Fig. 4, but instead of plotting against pump current or RIN, $\Delta f_{\mathrm{ceo}}$ is plotted against $S_{\mathrm{ceo}}$ values that were also recorded for each RIN setting. The linewidth is taken as the FWHM of the field spectrum of a signal, $\exp(\mathrm{i}(2\pi ft + \varphi(t))$, where $\varphi(t)$ is the phase with a noise PSD of $S_f/\nu^2$. For white frequency noise that does not experience a roll-off, $\Delta f_{\mathrm{ceo}} = \pi S_{\mathrm{ceo}}(0)$ Hz. This is shown as the (upper) gray trace in Fig. 10. We see that the calculated linewidths based on white frequency noise ($\nu_{3\,\mathrm{dB}} \to \infty$) far exceed the measured $\Delta f_{\mathrm{ceo}}$ values. The reason for this discrepancy is that the frequency noise is not white; it rolls off at the characteristic frequency $\nu_{3\,\mathrm{dB}}$. The field spectrum for this frequency noise must be calculated numerically from a general expression (for example, see [27]). Alternatively, as is done here, we use a Monte Carlo approach to generate the field spectrum for such a frequency noise power spectral density.

After incorporating the roll-off observed in the fs-laser's FM behaviour we generate the lower black trace in Fig. 10. This trace shows good agreement with the measured $\Delta f_{\mathrm{ceo}}$ vs. $S_{\mathrm{ceo}}(0)$ values. (In addition, the inset of Fig. 9 shows a comparison between the calculated and measured field spectra, indicating that the shape of the field spectrum is dominated by the pump-induced frequency noise and not any residual frequency noise from environmental contributions.) The deviation at lower-frequency noise occurs because of the contribution of the white frequency noise floor. We also note that when $\nu_{3\,\mathrm{dB}} < S_n(0)$, as is the case for the free-running offset frequency, $\Delta f_{\mathrm{ceo}}$ can be approximated by the following expression:

$$\Delta f_{\mathrm{ceo}} \sim \pi (S_{\mathrm{ceo}}(0)\nu_{3\,\mathrm{dB}})^{1/2} . \tag{5}$$

This result can also be reached by approximating the PSD as a step function and using the analytical results of [28]. The roll-off of the laser response at the characteristic $\nu_{3\,\mathrm{dB}}$ frequency is critical to the comb performance; without it the frequency noise would extend to much higher Fourier frequencies and have a dramatic effect on the linewidth.

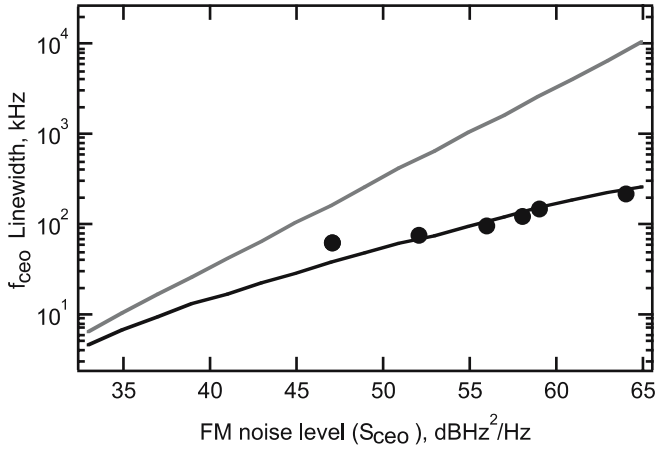


**FIGURE 10** FWHM line width of $f_{\mathrm{ceo}}$ vs. the one-sided power spectral density in frequency noise units. *Black line*: numerically calculated linewidth for a 7-kHz roll-off. *Gray line*: calculated linewidth for an infinite roll-off ($= \pi S_{\mathrm{ceo}}$). *Solid markers*: measured linewidths, $\Delta f_{\mathrm{ceo}}$, vs. measured frequency noise, $S_{\mathrm{ceo}}(0)$

## 4 Comb noise

Experimentally, we have so far established a relationship between the frequency noise of both $f_{\mathrm{r}}$ and $f_{\mathrm{ceo}}$ and the pump laser RIN. We are generally more interested in the linewidth and frequency noise of the components across the comb. As mentioned above, the noise on $f_{\mathrm{r}}$ and $f_{\mathrm{ceo}}$ will be linearly correlated. From the standard comb equation (with the offset frequency subtracted for convenience) the frequency of the $n$th mode is

$$f_n = n f_{\mathrm{r}} - f_{\mathrm{ceo}} . \tag{6}$$

The $n$th comb element will be immune to pump power variations when $\mathrm{d}f_n/\mathrm{d}P = 0$. Subsequently,

$$n_{\mathrm{fix}} = \left(\frac{\mathrm{d}f_{\mathrm{ceo}}}{\mathrm{d}P}\right) \Big/ \left(\frac{\mathrm{d}f_{\mathrm{r}}}{\mathrm{d}P}\right) , \tag{7}$$

where $n_{\mathrm{fix}}$ represents the comb tooth that is stationary with respect to intensity fluctuations, i.e. the fixed point [15, 26]. Based on the measurements above, we find $n_{\mathrm{fix}} = 4.1 \times 10^6$. With $f_{\mathrm{r}} = 49.3$ MHz the wavelength of the fixed comb element is $1.48\ \mu\mathrm{m} \pm 2\%$, somewhat shorter than the centre wavelength of the laser's optical spectrum of $1.56\ \mu$m (the 2% uncertainty arises from the uncertainty associated with the measurements of $\mathrm{d}f_{\mathrm{ceo}}/\mathrm{d}P$ and $\mathrm{d}f_{\mathrm{r}}/\mathrm{d}P$). For the $f_{\mathrm{r}} = 50.1$ MHz setup, we also find $n_{\mathrm{fix}} = 4.1 \times 10^6$, giving the fixed point of the comb at $1.46\ \mu\mathrm{m} \pm 2\%$ [16].

Having a comb element whose frequency is fixed with respect to pump intensity fluctuations implies that the intensity noise drives a breathing-mode motion of the comb about this comb frequency. It then follows that the noise spectral density of a given comb element that arises solely from the pump intensity noise is

$$S_n(\nu) = (n - n_{\mathrm{fix}})^2 S_{\mathrm{r}}(\nu) , \tag{8}$$

where $S_n(\nu)$ is the spectral density of the frequency noise of the $n$th comb element and $S_{\mathrm{r}}(\nu)$ is that of the fundamental repetition rate signal. If we combine (8) with a generalized form of (5), we find that the FWHM linewidth increases linearly with $n$, or equivalently with optical frequency, as one moves away from the fixed point. If we incorporate noise arising from cavity-length fluctuations (e.g. through vibration and temperature changes) a more complete expression is

$$S_n(\nu) = (n - n_{\mathrm{fix}})^2 S_{\mathrm{r\_RIN}}(\nu) + n^2 S_{\mathrm{r\_CL}}(\nu) , \tag{9}$$

where $S_{\mathrm{r\_RIN}}$ is the noise on $f_{\mathrm{r}}$ arising from pump RIN and $S_{\mathrm{r\_CL}}$ is the noise arising from cavity-length fluctuations

(there is also a fixed comb element associated with $S_{r\_CL}$, but it will be close to zero [14] and is neglected here). There are additional contributions from the amplified spontaneous emission generated in the fiber gain medium (the quantum-limit contribution) mentioned above that we do not include here [25].

To support the authenticity of this equation, measurements of $S_n(\nu)$ have been made for a series of comb wavelengths: 1064, 1550, 1536 nm, and the offset frequency signal (for which $n = 0$). Below we use the alternative notation of $S_\lambda$ instead of $S_n$ to denote the frequency noise at the comb line near $\lambda$. Free-running, narrow linewidth cw lasers at the respective wavelengths have been combined with the comb to generate rf beat signals, for which the frequency noise is measured. The various frequency noise spectra are plotted in Fig. 11. For both $f_{ceo}$ and $f_{1064}$ the pump-induced noise clearly dominates the frequency noise spectra. For $f_{1536}$ and $f_{1550}$ the pump-induced noise is considerably smaller since these wavelengths are nearer the fixed point. In these cases the frequency noise PSD has contributions from the variations in the femtosecond laser cavity (characterized by $S_{r\_CL}$ in (9)) and from the frequency noise on the cw lasers themselves (in particular the 1536-nm laser). Nevertheless, by comparing the frequency noise at high and low currents we can see a contribution from the pump-induced frequency noise for both $S_{1536}$ and $S_{1550}$. Comparing Fig. 11c and d, we see a more significant fall in frequency noise for the 1550-nm beat than for the 1536-nm beat as the RIN is reduced. We attribute this to the 1536-nm cw laser having more noise than the 1550-nm laser. Note that the expected difference in the noise level between the 1550-nm and 1536-nm traces is only 1.1 dB when laser RIN dominates (due to different frequency separations from $f_{fix}$).

Figure 12 shows the directly measured noise spectral densities of beat signals for two different pump current settings: 400 mA (black diamonds) and 1000 mA (purple circles). These data are taken from the upper- and lower-most traces of each plot in Fig. 12. The data points at the extrema

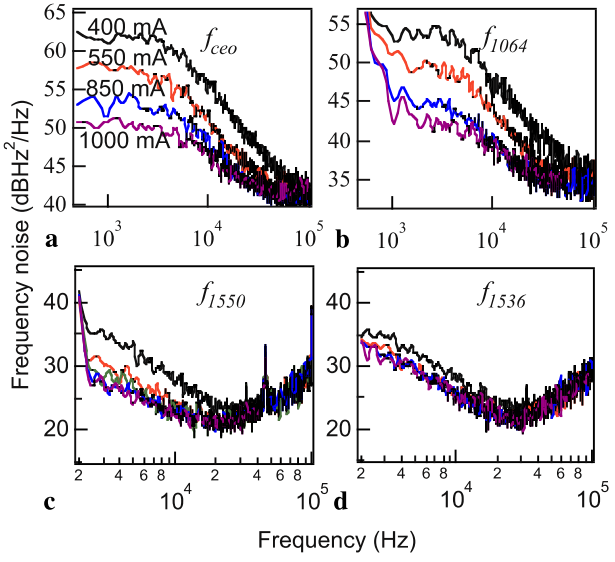


**FIGURE 11** Frequency noise spectra ($S_\lambda$) at three comb wavelengths; 1064 nm, 1536 nm, 1550 nm, and for $f_{ceo}$ for four different pump currents ($f_r = 50.1$ MHz)

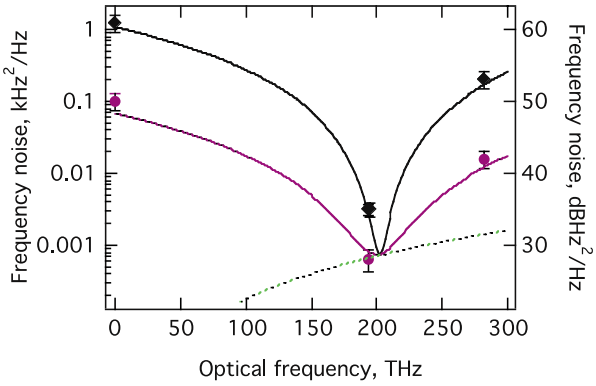


**FIGURE 12** Frequency noise recorded at specific comb wavelengths, compared to theoretical traces produced by (9). Two widely separated RIN levels are considered; 400 mA (*black diamonds* and *black trace*) and 1000 mA (*purple circles* and *purple trace*). The *green dashed line* is the calculated resultant noise arising from cavity-length fluctuations alone at $\nu = 3$ kHz

show the level of white FM noise below the roll-off frequency for $f_{ceo}$ and 1064-nm beat signals (0 THz and 282 THz, respectively). The noise spectra $S_{1536}$ and $S_{1550}$ do not exhibit white frequency noise, so the noise at a convenient Fourier frequency, $\nu = 3$ kHz, is considered. Also shown are the theoretical curves calculated using (9) (black and purple lines) with RIN levels associated with the two pump current levels. If we were to discard the cavity-length fluctuations, as in (8), the model traces would plunge toward zero as the frequency approaches that of the fixed point. However, including a estimate of the environmental contribution ($S_{r\_CL}$ of (9)), shown as the green dashed line in Fig. 12, puts a lower limit on the frequency noise (again at $\nu = 3$ kHz). A direct measurement of $S_{r\_CL}$ at 3 kHz is difficult to make. In practice the noise of the phase reference (e.g. a microwave synthesizer) inundates that of $f_r$. Instead we make the assumption that the 1550-nm beat signal noise at 1000 mA (and 3 kHz) is dominated by $S_{r\_CL}$ contributions; then we find $S_{r\_CL} \sim 5 \times 10^{-11}$ Hz$^2$/Hz at this Fourier frequency. We can treat this as an upper estimate, since it is possible that $S_{1550}$ contains a contribution from the cw laser itself. However, the quoted value for $S_{r\_CL\_3\,kHz}$ is consistent with a $\sim 5 \times 10^{-4}/f^2$ Hz$^2$/Hz slope derived from phase noise measurements of $f_r$ below $\nu = 1$ kHz (measured with the lowest RIN). The calculated traces based on (9) and the measured data agree well across the broad optical frequency range considered ($S_{1536}$ at 1 A has been omitted since it does not represent comb noise).

To continue the quantitative analysis we compare, in ratio terms, the power spectral density of $f_{ceo}$ to that of a beat signal at a particular comb wavelength ($S_\lambda$), in this case at 1064 nm. From (9) the ratio of $S_{ceo}$ to $S_\lambda$ is computed to be

$$\frac{S_{ceo}}{S_\lambda} = \frac{n_{fix}^2}{(n_\lambda - n_{fix})^2 + n_\lambda^2 S_{r\_CL}(\nu)/S_{r\_RIN}(\nu)}. \tag{10}$$

The second term in the denominator is typically small. At 1064 nm and the lowest RIN values it is $\sim 10\%$ of the first term. Ignoring it, (10) simplifies to

$$\frac{S_{ceo}}{S_\lambda} = \frac{n_{fix}^2}{(n_{fix} - n_\lambda)^2} = \frac{f_{fix}^2}{(f_{fix} - f_\lambda)^2}. \tag{11}$$

| $I_{\text{pump}}$ [1] (mA) | $\overline{S_{\text{ceo}}/S_{1064}}$ lin. units | S. dev. | $I_{\text{pump}}$ [2] (mA) | $\overline{S_{\text{ceo}}/S_{1064}}$ lin. units | S. dev. |
|---|---|---|---|---|---|
| 320 | 8.86 | 2.45 | 400 | 5.92 | 1.51 |
| 520 | 5.78 | 2.12 | 550 | 5.23 | 1.07 |
| 700 | 5.73 | 1.73 | 700 | 6.46 | 1.79 |
| 830 | 6.43 | 1.85 | 850 | 6.66 | 1.55 |
| 950 | 5.34 | 1.63 | 1000 | 5.60 | 1.35 |
| Mean | 6.15 | 0.88 | | 5.80 | 0.66 |

[1] $f_{\text{r}} = 49.3$ MHz, $S_{\text{ceo}}$ data from Fig. 5
[2] $f_{\text{r}} = 50.1$ MHz, $S_{\text{ceo}}$ and $S_{1064}$ data from Fig. 11

**TABLE 1** A summary of the mean frequency noise ratio between the $f_{\text{ceo}}$ and 1064-nm beat signals for a range of pump currents, and for two slightly different length fs-laser cavities (1 kHz $< \nu <$ 15 kHz)

In formulating the right-most term, the effect of $f_{\text{ceo}}$ in (6) is negligible, so it does not appear in the expression. Frequency noise spectra for $f_{\text{ceo}}$ are shown in Figs. 5 and 11 for two slightly different length cavities ($f_{\text{r}} = 49.3$ MHz and 50.1 MHz, respectively). Measurements of $S_{1064}$ were also recorded for both cavities; noise spectra for the 50.1-MHz laser appearing in Fig. 11. Each ratio of the spectral densities was evaluated over the 1 kHz to 15 kHz frequency range and the mean values and standard deviations deduced for a series of pump laser current settings. These are summarized in Table 1. The final row expresses the weighted mean of the noise ratios, along with the mean standard deviation added in quadrature.

From the tabulated data of the 49.3-MHz laser we see that

$$\frac{S_{\text{ceo}}}{S_{1064}} = 6.15 \pm 0.88\,, \tag{12}$$

while the right-hand side of (10) is calculated to fall within 5.85 and 6.35 depending on the value of $S_{\text{r\_RIN}}$, which can range from $6.5 \times 10^{-9}$ to $65 \times 10^{-9}$ Hz$^2$/Hz given the pump laser RIN variation found in Fig. 3 (and which applies to the $S_{\text{ceo}}$ and $S_{1064}$ measurements here). The measured mean noise ratio of 6.15 lies close to the centre of this range. If we were to assume the simpler expression of (11) we find $S_{\text{ceo}}/S_{1064} = 6.4 \pm 0.6$, slightly higher than the measured ratio but close nonetheless. This last result validates the use of (8), since it can be used to derive (11).

Applying the same analysis to the noise spectra of Fig. 11a and b ($f_{\text{r}} = 50.1$ MHz) produces $S_{\text{ceo}}/S_{1064} = 5.80 \pm 0.66$. The same noise ratio calculated using (10) places it in the range of 6.5 to 7.1 depending on $S_{\text{r\_RIN}}$. If we include the uncertainty associated with $n_{\text{fix}}$, this range increases to 5.7–8.1, demonstrating that the measured and predicted values agree within the measurement uncertainties. Note that a 2% change in $n_{\text{fix}}$ causes a 13% change in $S_{\text{ceo}}/S_{1064}$.

## 5 Eliminating pump-induced frequency jitter

An advantage of reducing the free-running noise on the carrier-envelope offset frequency signal is that the excess noise can now be suppressed to such an extent as to leave the $f_{\text{ceo}}$ signal with very low residual phase noise when phase locked to a rf signal. The servo bandwidth controlling $f_{\text{ceo}}$ has been extended well beyond the $\nu_{3\,\text{dB}}$ response bandwidth of the femtosecond laser by employing phase-lead compensation [29] of the correction signal sent to the current-modulation port of the pump laser. This approach relies on the fact that the fs laser exhibits a simple low-pass filter response to pump changes and does not exhibit relaxation oscillations. Figure 13 shows the resulting in-loop frequency noise spectrum. The servo bumps occur approximately 80 kHz from the carrier, indicating the breadth of the servo bandwidth. This limit is a result of accumulated phase shifts within the current-modulation circuit for the pump diode, and servo.

An example of the field spectrum of $f_{\text{ceo}}$ under phase-locked conditions is shown in Fig. 14. The coherent peak is clearly present with an instrument-limited full width half-maximum (resolution bandwidth = 0.3 Hz). Similar narrow linewidth $f_{\text{ceo}}$ beats have been observed by Hartl et al. [5, 18] that relied on a saturable absorber based mode-locked fiber laser.

Once a coherent peak is achieved, the concept of the FWHM linewidth is less useful and should be replaced by an analysis of the phase noise. The integrated phase noise from the data of Fig. 14 is calculated as

$$\delta\varphi^2_{\text{ceo}} = \int_0^{500\ \text{kHz}} \nu^{-2} S_{\text{ceo}}(\nu)\,\mathrm{d}\nu = 0.99\ \text{rad}^2\,. \tag{13}$$

The pulse-to-pulse phase jitter will have added contributions from any white phase noise floor that extends out to the

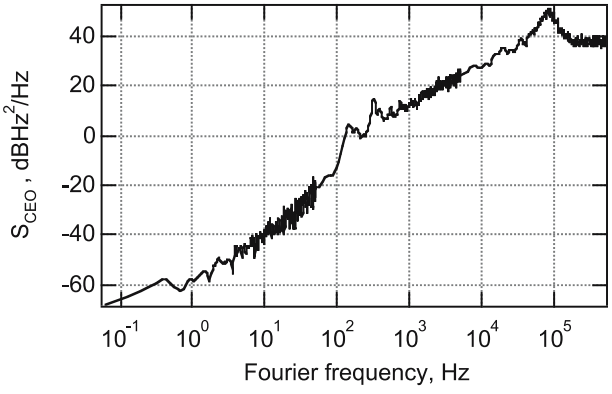


**FIGURE 13** In-loop frequency noise spectrum of the phase-locked $f_{\text{ceo}}$ signal

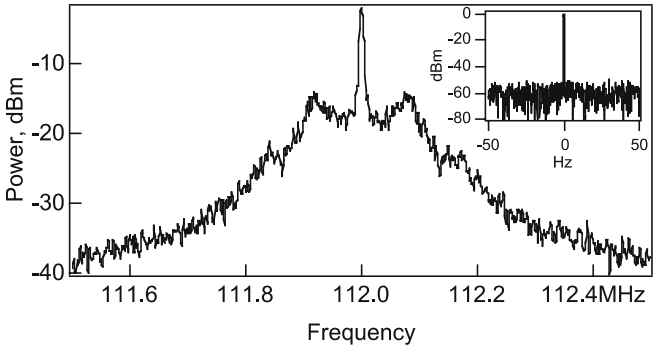


**FIGURE 14** Field spectrum of the phase-locked $f_{\text{ceo}}$ beat at 3-kHz resolution bandwidth. *Inset*: phase-locked $f_{\text{ceo}}$ beat at 0.3-Hz resolution bandwidth and centre frequency offset to 0 Hz

Nyquist frequency of 25 MHz. However, simple extrapolation of the present $-75$ dB rad$^2$/Hz white phase noise floor out to 25 MHz gives a pulse-to-pulse phase jitter on the CEO phase of only 1.3 rad. This very low jitter on the CEO phase yields a lot of promise for future measurements with the frequency comb that depend on the carrier-envelope phase.

## 6 Conclusions

A significant source of frequency noise in a fiber-based frequency comb has been identified, namely the intensity noise of a Bragg grating stabilized semiconductor laser pumping the mode-locked fiber laser. The influence of the pump laser's intensity noise has been characterized by measuring noise spectra of beat signals at several comb wavelength locations, including the carrier-envelope offset frequency beat, for different levels of pump laser RIN (without affecting the pump power acting on the fiber laser). A reduction in RIN shows a dramatic reduction in comb noise, particularly in the wings of the frequency comb where, through the breathing motion of the comb about a fixed point, the noise is the most manifest. A model incorporating the fiber laser intensity noise and the breathing effect of the comb adheres closely to experimental results. By lowering the pump laser RIN, the field spectrum linewidth of the free-running CEO frequency signal has been lowered from several hundred kHz to $\sim 60$ kHz.

By exploiting the simple low-pass filter response of the femtosecond fiber laser, we are able to significantly extend the feedback bandwidth for the pump laser control from $\sim 5$ kHz to 80 kHz. This increased bandwidth permits a very tight phase lock of $f_{\mathrm{ceo}}$ to the reference rf oscillator. The residual in-loop phase excursions have been shown to be as low as 1 rad for frequencies integrated out to 500 kHz. Extrapolating out to the Nyquist frequency gives $\sim 1.3$ rad of phase noise. Further decreases in the pump RIN and even more aggressive phase-lead compensation could reduce this phase jitter even further. This tight phase lock of $f_{\mathrm{ceo}}$ has important consequences for frequency metrology, since the counted $f_{\mathrm{ceo}}$ beat exhibits frequency variations $\leq 1$ mHz in a 1-s gate time under these conditions. The corresponding statistical error in the counted optical frequency is $1\,\mathrm{mHz}/200\,\mathrm{THz} < 10^{-17}$. Furthermore, the low phase jitter could enable time-domain experiments with the fiber laser frequency comb similar to those being pursued with Ti:sapphire frequency combs [30].

**ACKNOWLEDGEMENTS** We are grateful for the loan of equipment from I. Vayshenker and T. Clement, for helpful discussions with S. Diddams and L. Hollberg, and for assistance from I. Coddington and S. Etzel. J.J.M. thanks the Australian Research Council for travel funding (through E. Ivanov and A. Luiten). This work was partially funded under the DARPA PHOR-FRONT program.

## REFERENCES

1 F.-L. Hong, K. Minoshima, A. Onae, H. Inaba, H. Takada, A. Hirai, H. Matsumoto, T. Suguira, M. Yoshida, Opt. Lett. **28**, 1516 (2003)
2 F. Tauser, A. Leitenstorfer, W. Zinth, Opt. Express **11**, 594 (2003)
3 B.R. Washburn, S.A. Diddams, N.R. Newbury, J.W. Nicholson, M.F. Yan, C.G. Jorgensen, Opt. Lett. **29**, 250 (2004)
4 T.R. Schibli, K. Minoshima, F.-L. Hong, H. Inaba, A. Onae, H. Matsumoto, I. Hartl, M.E. Fermann, Opt. Lett. **29**, 2467 (2004)
5 I. Hartl, G. Imeshev, M.E. Fermann, C. Langrock, M.M. Fejer, Opt. Express **13**, 6490 (2005)
6 J. Rauschenberger, T. Fortier, D. Jones, J. Ye, S. Cundiff, Opt. Express **10**, 1404 (2002)
7 H. Hundertmark, D. Wandt, C. Fallnich, N. Haverkamp, H.R. Telle, Opt. Express **12**, 770 (2004)
8 K. Moutzouris, F. Adler, F. Sotier, D. Trautlein, A. Leitenstorfer, Opt. Lett. **31**, 1148 (2006)
9 F. Adler, K. Moutzouris, A. Leitenstorfer, H. Schnatz, B. Lipphardt, G. Grosche, F. Tauser, Opt. Express **12**, 5872 (2004)
10 B.R. Washburn, R.W. Fox, N.R. Newbury, J.W. Nicholson, K. Feder, P.S. Westbrook, C.G. Jorgensen, Opt. Express **12**, 4999 (2004)
11 P. Kubina, P. Adel, F. Adler, G. Grosche, T.W. Hänsch, R. Holzwarth, A. Leitenstorfer, B. Lipphardt, H. Schnatz, Opt. Express **13**, 904 (2005)
12 W.C. Swann, N.R. Newbury, Opt. Lett. **31**, 826 (2006)
13 B.R. Washburn, W.C. Swann, N.R. Newbury, Opt. Express **13**, 10622 (2005)
14 N.R. Newbury, B.R. Washburn, IEEE J. Quantum Electron. **QE-41**, 1388 (2005)
15 E. Benkler, H. Telle, A. Zach, F. Tauser, Opt. Express **13**, 5662 (2005)
16 J.J. McFerran, W.C. Swann, B.R. Washburn, N.R. Newbury, Opt. Lett. **31**, 1997 (2006)
17 K. Tamura, H.A. Haus, E.P. Ippen, L.E. Nelson, Opt. Lett. **18**, 1080 (1993)
18 I. Hartl, G. Imeshev, G.C. Cho, M.E. Fermann, K. Minoshima, A. Onae, F.-L. Hong, H. Matsumoto, J.W. Nicolson, M.F. Yan, in *Trends in Optics and Photonics, Advanced Solid-State Photonics*, ed. by G.J. Quarles (Optical Society of America, Washington, DC, 2004), pp. 176–178
19 H.A. Haus, K. Tamura, L.E. Nelson, E.P. Ippen, IEEE J. Quantum Electron. **QE-31**, 591 (1995)
20 J.W. Nicholson, P.S. Westbrook, K.S. Feder, A.D. Yablon, Opt. Lett. **29**, 2363 (2004)
21 J.H. Shoaf, D. Halford, A.S. Risley, NBS Tech. Note **632**, 40 (1973)
22 Y. Ohki, N. Hayamizu, S. Irino, H. Shimizu, J. Yoshida, N. Tsukiji, Furukawa Rev. **24**, 6 (2003)
23 H.A. Haus, A. Mecozzi, IEEE J. Quantum Electron. **QE-29**, 983 (1993)
24 R. Paschotta, Appl. Phys. B **79**, 163 (2004)
25 R. Paschotta, A. Schlatter, S.C. Zeller, H.R. Telle, U. Keller, Appl. Phys. B **82**, 265 (2006)
26 H.R. Telle, B. Lipphardt, J. Stenger, Appl. Phys. B **74**, 1 (2002)
27 D.R. Hjelme, A.R. Mickelson, R.G. Beausoleil, IEEE J. Quantum Electron. **QE-27**, 352 (1991)
28 D.S. Elliott, R. Roy, S.J. Smith, Phys. Rev. A **26**, 12 (1982)
29 M. Ohtsu, *Highly Coherent Semiconductor Lasers* (Artec House, Boston London, 1992), p. 317
30 A. Baltuska, T. Udem, M. Uiberacker, M. Hentschel, E. Goulielmakis, C. Gohle, R. Holzwarth, V.S. Yakovlev, A. Scrinzl, T.W. Hänsch, F. Krausz, Nature **421**, 611 (2003)